DUROMETER HARDNESS AND THE STRESS-STRAIN BEHAVIOR OF ELASTOMERIC MATERIALS

H. J. QI, K. JOYCE, M. C. BOYCE*

DEPARTMENT OF MECHANICAL ENGINEERING
MASSACHUSETTS INSTITUTE OF TECHNOLOGY, CAMBRIDGE, MA 02139

ABSTRACT

The Durometer hardness test is one of the most commonly used measurements to qualitatively assess and compare the mechanical behavior of elastomeric and elastomeric-like materials. This paper presents nonlinear finite element simulations of hardness tests which act to provide a mapping of measured Durometer Shore A and D values to the stress-strain behavior of elastomers. In the simulations, the nonlinear stress-strain behavior of the elastomers is first represented using the Gaussian (neo-Hookean) constitutive model. The predictive capability of the simulations is verified by comparison of calculated conversions of Shore A to Shore D values with the guideline conversion chart in ASTM D2240. The simulation results are then used to determine the relationship between the neo-Hookean elastic modulus and Shore A and Shore D values.

The simulation results show the elastomer to undergo locally large deformations during hardness testing. In order to assess the potential role of the limiting extensibility of the elastomer on the hardness measurement, simulations are conducted where the elastomer is represented by the non-Gaussian Arruda-Boyce constitutive model. The limiting extensibility is found to predict a higher hardness value for a material with a given initial modulus. This effect is pronounced as the limiting extensibility decreases to less than 5 and eliminates the one-to-one mapping of hardness to modulus. However, the durometer hardness test still can be used as a reasonable approximation of the initial neo-Hookean modulus unless the limiting extensibility is known to be small as is the case in many materials, such as some elastomers and most soft biological tissues.

INTRODUCTION

Durometer (Shore) hardness[1] is one of the most commonly used hardness tests for elastomeric materials. Durometer hardness measurements, which assess the material resistance to indentation, are widely used in the elastomer industry for quality control and for quick and simple mechanical property evaluation.[1] The hardness value is primarily a function of the elastic behavior of the material. The nondestructive and relatively portable nature of the test enables property evaluation directly on elastomeric products or components. This feature has also led to the use of hardness tests in mechanical property evaluation of soft tissues such as skin[3-4] and tumors surrounded by soft tissues.[5]

Durometer hardness is related to the elastic modulus of elastomeric materials. Several theoretical efforts have been conducted in the past to establish the relationship between hardness and elastic modulus.[6-7] However, most of these efforts have been based on linear elasticity, even though the indentation in durometer hardness tests involves significant large-scale nonlinear deformation. Gent[6] obtained a simple relation between the elastic modulus and durometer Shore A hardness by approximating the truncated cone indentor geometry as a cylinder and using the classic linear elastic solution for the flat punch contact problem. Briscoe and Sebastian[7] considered the actual shape of the Shore A indentor and linear elasticity theory to obtain a prediction using an iterative solution. The difference between the Gent and the Briscoe and Sebastian results was as large as 15% to 25% for durometer hardness values larger than 50A. In this paper, the ability of durometer Shore hardness tests to provide properties for the stress-strain behavior of elastomers for small to large deformation is assessed. Fully nonlinear finite element analyses are conducted to simulate the durometer hardness tests. The nonlinear stress-strain behavior of the materials is modeled using the Gaussian (neo-Hookean) model and the Arruda-Boyce eight-

* Corresponding author. Ph: 1-617-253-2342; Fax: 1-617-258-8742; email: mcboyce@mit.edu

chain non-Gaussian model. The latter constitutive model captures the limiting extensibility of elastomers (and also of soft tissues[8]) and thus permits evaluation of the relevance of correlating the durometer measurements to limiting aspects of material behavior. Durometer tests for Shore A and Shore D scales are simulated for the Gaussian (neo-Hookean) material. The ability of the model to predict the corresponding Shore D hardness for a given Shore A hardness material acts as a verification. A mapping of Shore A and D values to the elastic modulus predictions is then provided. Comparisons of the new model with prior models are also given. The influence of the limiting extensibility of elastomeric materials on this mapping is assessed.

MODELS

THE MODEL OF DUROMETER HARDNESS TESTS

The durometer hardness test is defined by ASTM D 2240,[1] which covers seven types of durometer: A, B, C, D, DO, O, and OO. Table I shows the comparison of different durometer scales.

TABLE I
COMPARISON OF DIFFERENT SCALES OF DUROMETER TESTS

Type A	10 20 30 40 50 60 70 80 90 100
Type B	10 20 30 40 50 60 70 80 90 100
Type C	10 20 30 40 50 60 70 80 90 100
Type D	10 20 30 40 50 60 70 80 90 100
Type DO	10 20 30 40 50 60 70 80 90 100
Type O	10 20 30 40 50 60 70 80 90 100
Type OO	10 20 30 40 50 60 70 80 90 100

Most commercially available products for durometer tests consist of, according to ASTM D 2240, four components: presser foot, indentor, indentor extension indicating device, and calibrated spring, as shown in Figure 1. The scale reading is proportional to the indentor movement (Figure 2)

$$H = \frac{\Delta L}{0.025mm}, \ \Delta L = L_0 - L \tag{1}$$

where H is the hardness reading; ΔL is the movement of the indentor.

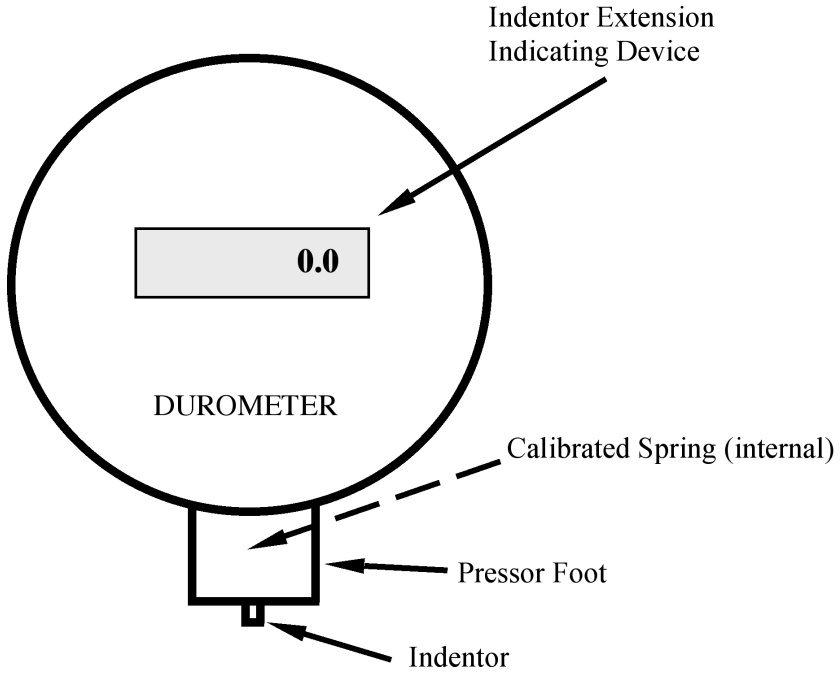

FIG. 1. — A typical durometer.

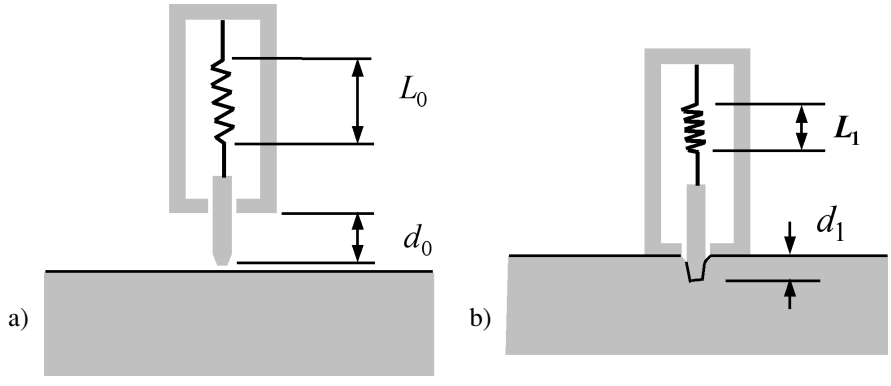

FIG. 2. — Schematics of the working mechanism of durometers.
(a) Before the durometer is pressed down; (b) the durometer is pressed down.

A durometer essentially measures the reaction force on the indentor through the calibrated spring when it is pressed into the material. The relation between the force measured and the movement of the indentor is

$$F = 0.55 + 3\Delta L \tag{2a}$$

for type A, B and O durometers; and

$$F = 17.78\Delta L \tag{2b}$$

for type C, D and DO durometers.

In durometer tests, as the durometer is pressed onto the specimen surface, the indentor penetrates into the specimen, and is simultaneously pressed up into the device as well. This process is depicted in Figure 2, where L_0 is the free length of the calibrated spring; d_0 is the distance between the indentor tip and the presser foot lower surface and according to ASTM D 2240, d_0 = 2.5 mm; d_1 is the corresponding distance in the fully loaded condition. Since the lower surface of the presser foot is always in contact with the specimen surface when the reading is taken, it is straightforward to obtain (Figure 2)

$$\Delta L + (d_1 - 0) = 2.5 \tag{3}$$

The indentor is in equilibrium, therefore

$$F_r(h)\Big|_{h=d_1} = F \tag{4}$$

where F_r is the reacting force of the elastomeric specimen due to the indentor penetration denoted by h. Therefore, the objective equations relating the hardness measurement to the stress-strain behavior of the elastomers consist of Equation (3) and Equation (4). The exact form of $F_r(h)$ however is unknown. Gent[6] used the linear elastic Hertz contact solution for the case of a simplified indentor shape. Briscoe and Sebastian[7] considered the actual geometry of the indentor. This method however requires computationally cumbersome numerical methods for the solution. In this paper, we take advantage of developments in nonlinear finite element method (FEM) and numerically simulate the hardness tests to obtain $F_r(h)$ in the form of a force vs indentation, F vs h, curve. The hardness scale reading is then obtained by finding the intercept point as shown in Figure 3.

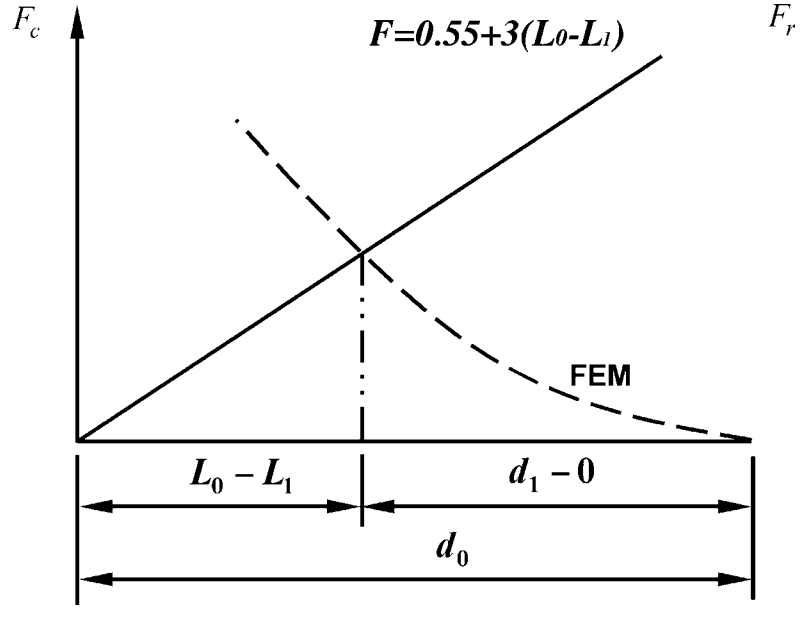

FIG. 3. — Schematic of the method to obtain durometer readings.

FEM MODELS FOR INDENTATION SIMULATIONS

Geometry. — The force vs indentation curve is obtained using a fully nonlinear finite element simulation of the indentation test. Since the indentors have axially symmetric cross sections, it is effective to model the problem as an axisymmetric one. As shown in Figure 4, the vertical boundary AD is subjected to the axisymmetric boundary condition, $u_r|_{\mathrm{AD}} = 0$. In order to reduce the influence from the specimen boundary, ASTM D 2240 requires that the test specimen should be at least 6 mm in thickness and the locus of indentation should be at least 12 mm away from any edges. Therefore, in Figure 4, $AB = 15mm$, $BC = 8\ mm$. Due to the existence of friction, the lower surface AB of the specimen cannot move freely along the horizontal direction, $u_r|_{AB} = u_z|_{AB} = 0$.

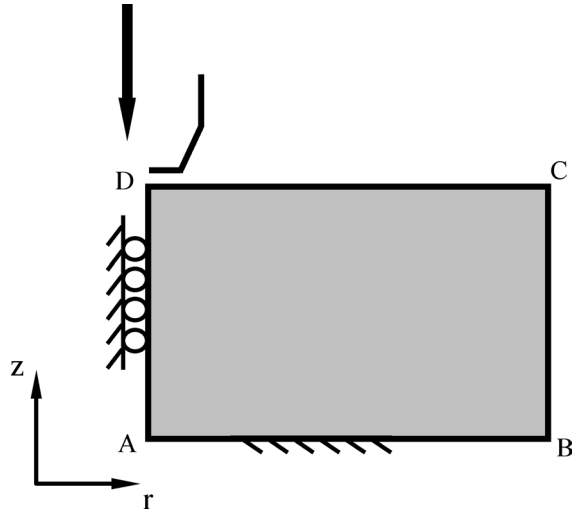

FIG. 4. — The finite element method model for simulations of indentation.

The boundary value problem is solved using the finite element code ABAQUS. Axisymmetric 8-node, hybrid continuum elements with biquadratic interpolation of the displacement field and linear interpolation of pressure are used to model the elastomer. Figure 5 shows the mesh used for the durometer A analyses. The indentor is modeled as a rigid surface since it is much stiffer than the elastomers being tested. The mesh is refined in the vicinity of the contact region where large gradients in stress and strain prevail. Several mesh densities were analyzed and an optimal mesh was finally chosen for use in all simulations. For durometer D analyses, a similar mesh has been used with the exception of the shape of the indentor.

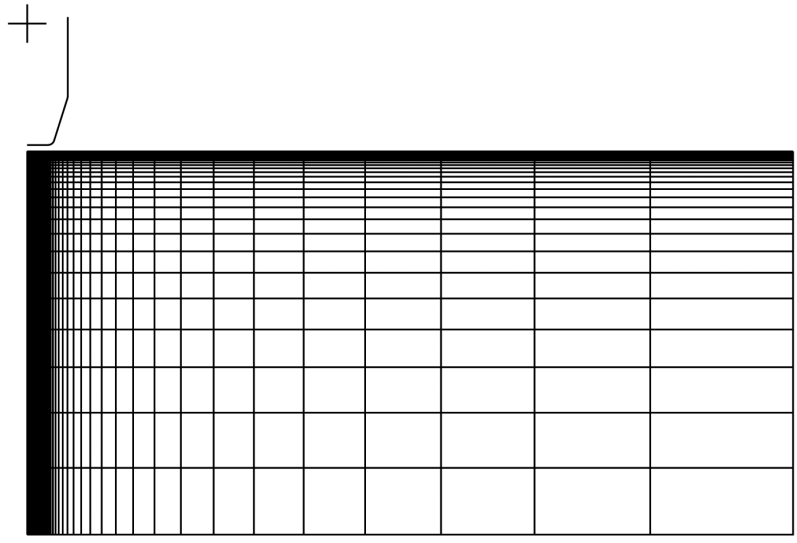

FIG. 5. — The mesh used for the FEM simulations.

The effect of friction on the simulation was studied by simulating selected cases of A-type and D-type tests using a friction coefficient of 0.3 between the indentor and the elastomer. Friction was found to increase the F vs h curve by no more than 4% in most cases. A similar result has been reported by Chang *et al.*[9] for indentation with a rigid ball. Therefore, friction was neglected with exception that in D type analyses a friction coefficient of 0.1 was used to reduce the large deformation experienced by the elements on the contact surface.

Material Model. — The rubber elasticity constitutive laws in the simulations are the Gaussian (neo-Hookean) model[10] and the Arruda-Boyce eight-chain model.[11] Both models are based on the concept of an elastomer as a three-dimensional network of long chain molecules, linked together at points of cross-linkage. The Gaussian model assumes Gaussian chain statistics to apply and the strain energy density function is given by

$$W_G = \frac{1}{2}\mu\left(\lambda_1^2 + \lambda_2^2 + \lambda_3^2 - 3\right) = \frac{1}{2}\mu\left(I_1 - 3\right) \qquad (5)$$

where $\mu = nk\Theta$; n is the number of chains per unit volume; k is Boltzmann's constant; Θ is absolute temperature; λ_1, λ_2, and λ_3 are the three principal stretches; and I_1 is the first invariant of the stretch $I_1 = \lambda_1^2 + \lambda_2^2 + \lambda_3^2$.

The limitation of the Gaussian theory is that as chains become highly stretched, the stress level is under-predicted, necessitating a non-Gaussian statistical theory to depict the behavior of the chain deformations approaching their limited extensibility. The Arruda-Boyce model employs a representative description of the network containing eight non-Gaussian chains extending from the center of a cube to each corner (see Figure 6) to simulate the network structure of the polymer. The initial chain length is, from random walk statistics, given by $r_0 = \sqrt{N}l$, where N is the number of rigid links of length l between the points of cross linkage. The maximum length of the chain is Nl and the maximum chain stretch, which is called the locking stretch

or limiting extensibility, is

$$\lambda_L = \frac{Nl}{r_0} = \sqrt{N} \tag{6}$$

The cube is deformed in the principal stretch space and the stretch of each chain in the network is

$$\lambda_{chain} = \frac{r_{chain}}{r_0} = \sqrt{\frac{I_1}{3}} \tag{7}$$

Note that the concept of the effective chain stretch λ_{chain} can also be applied to the Gaussian model. The strain energy density function for this 8-chain network is[11]

$$W_{AB} = \mu\left(\lambda_{chain}\sqrt{N}\beta + N\ln\frac{\beta}{\sinh\beta}\right) - \Theta c \tag{8}$$

where β is the inverse Langevin function, $\beta = L^{-1}\left[\lambda_{chain}/\sqrt{N}\right]$, and $L[\beta] = \coth\beta - (1/\beta)$, c is a constant.

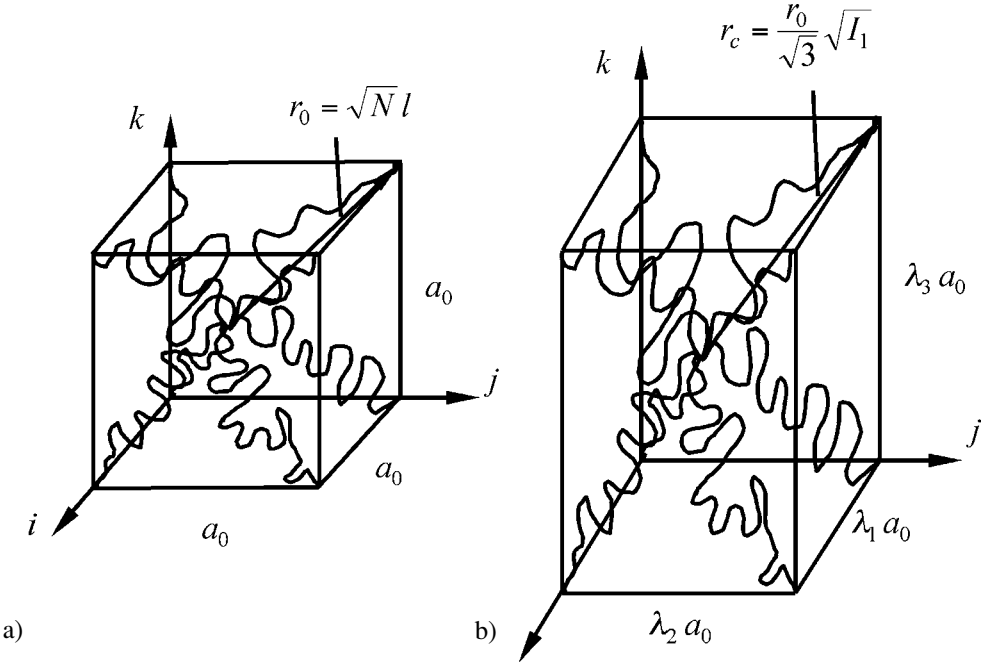

FIG. 6. — The network for the eight chain model: (a) unstretched state; (b) stretched state.

It can be shown that the initial elastic modulus of the material from a uniaxial tensile test is

$$E_0 = 3\mu \tag{9a}$$

for the Gaussian model and

$$E_0 = 3\mu\left(1 + \frac{40425}{67375N} + \frac{39501}{67375N^3} + \frac{42039}{67375N^4} + \ldots\right) \tag{9b}$$

for the Arruda-Boyce model using a power series expansion representative of the inverse Langevin function. Observe that the elastic modulus predicted by Gaussian model is independent of chain limiting extensibility. The difference between the initial moduli for the Arruda-Boyce model and the Gaussian model increases as N decreases or the crosslinking density increases; when N is 6, the difference is 10% and when N is 4, the difference is 16%.

RESULTS AND DISCUSSIONS

SIMULATIONS ON DUROMETER A AND DUROMETER D

Finite element simulations of representative durometer hardness tests are conducted for Gaussian materials with $\mu = 1.6MPa$ for a Shore A test and $\mu = 30MPa$ for a Shore D test, respectively.

In Figure 7, the force-indentation curve from the simulation of the Shore A test is depicted together with the spring behavior described earlier in Equation (2a). The Shore A hardness value is obtained by finding the intersection of these two curves, which occurs at an indentation depth of 1.00 mm, giving a Shore A value of 60A. Figure 8(a) and (b) show the contours of principal strain and chain stretch ratio λ_{chain} at the indentation depth of 1.00 mm, respectively. These contours reveal that the elastomer experiences modest to large strain for this representative case (the Shore A scale is commonly used to indicate the durometer of materials between 30A to 90A). The maximum chain stretch ratio is observed around the corner of the indentor tip and is 2.2. For elastomers with a low limiting extensibility, this result indicates that it may be necessary to consider this effect when relating durometer to nonlinear stress-strain behavior.

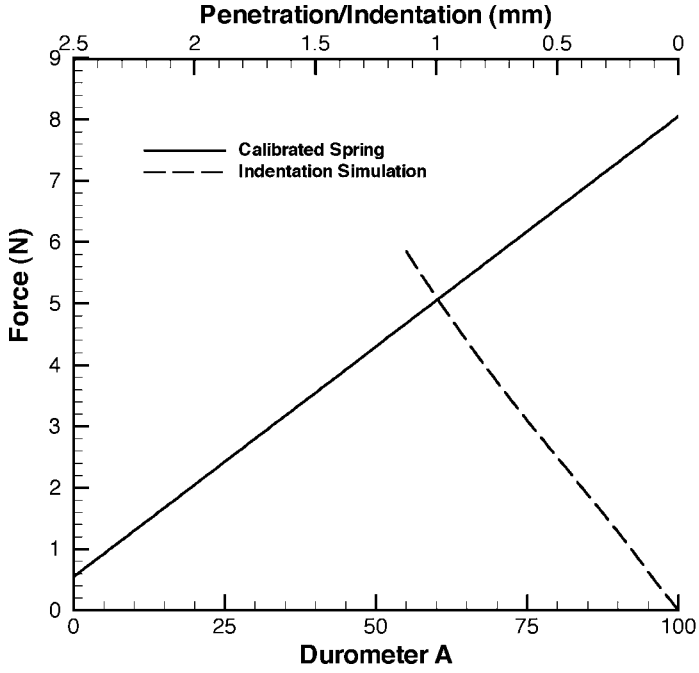

FIG. 7. — The solid line is the force-penetration curve for the calibrated spring following Equation (2a). Dashed line is the force-indentation curve from the Shore A test simulation for a Gaussian material with $\mu = 1.6\ MPa$.

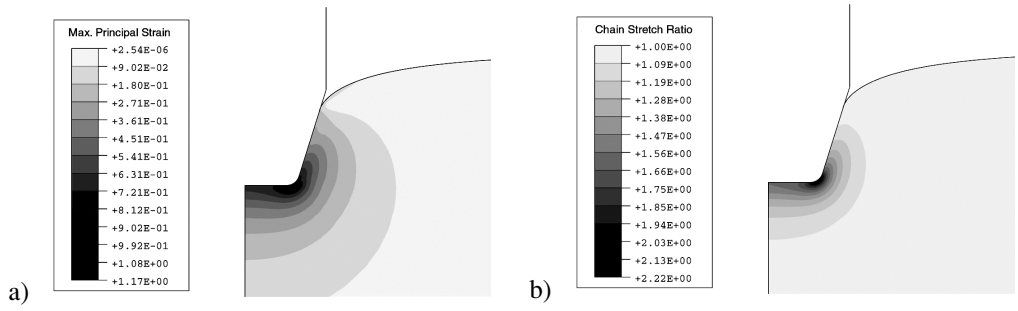

FIG. 8. — Results for Shore A simulation for the Gaussian material with $\mu = 1.6\ MPa$. (a) Contours of the maximum principal strain; (b) contours of the chain stretch ratio.

Similar to the Shore A case, the Shore D hardness value for the Gaussian material of $\mu = 30MPa$ is obtained by finding the intersection of the spring response of Equation (2b) and the force-indentation curve for Shore D hardness indentation. The Shore hardness for this material is 62D and the penetration is 0.95 mm. Figure 9(a) and (b) show the maximum principal strain contour and the chain stretch ratio contour, respectively, at the fully loaded indentation (0.95 mm) for this representative Shore D test. The strains are highly localized for this cone shape indentor and are rather high. The maximum chain stretch ratio is 9.5, and maximum principal strain is 3.9, suggesting that the limiting extensibility of the material may play an important role in evaluating material Shore hardness.

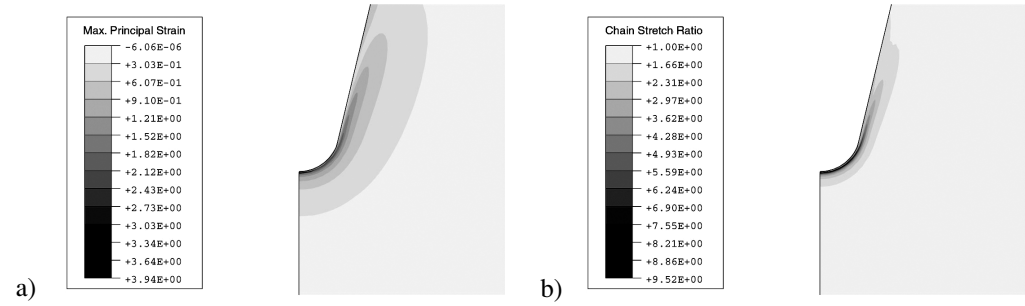

FIG. 9. — Results for Shore D simulation for the Gaussian material with $\mu = 30\ MPa$.
(a) Contours of the maximum principal strain; (b) Contours of the chain stretch ratio.

COMPARISONS BETWEEN SHORE A AND SHORE D

To verify the proposed method, the finite element simulations of durometer hardness tests for scale A and scale D were conducted for three Gaussian materials with $\mu = 3.3MPa$, $\mu = 6.0MPa$, $\mu = 9.2MPa$, respectively. The materials were chosen to provide durometer readings where the A and D scales overlap.

For the material with $\mu = 3.3MPa$, the predicted durometer hardness is 75A and 25D. According to the guideline comparison chart in ASTM D 2240,[1] the material with durometer hardness 75 in scale A should give a hardness of about 24 in scale D. Similar comparisons are made for materials with $\mu = 6.0MPa$, $\mu = 9.2MPa$ and are listed in Table II. It should be noted that the comparison chart in ASTM D 2240 is loosely defined and cannot be used for absolute comparison purposes. Indeed, conversions which differ slightly were found.[12] Therefore, although a relatively large error exists for 90A, Table II shows generally good agreement between simulated values and values from the comparison chart. This verifies the capability of the current finite element simulation to predict both A scale and D scale durometer hardness. The regions where direct conversions are not as reliable will be shown to occur at the tail end of the A scale where the relationship between the hardness and modulus becomes highly nonlinear.

TABLE II
COMPARISON OF SHORE A AND SHORE D HARDNESS BY SIMULATIONS. BOTH SHORE A AND SHORE D VALUES ARE OBTAINED FOR THE SAME MATERIALS BY FINITE ELEMENT METHOD SO THAT A CONVERSION BETWEEN A SCALE AND D SCALE IS ESTABLISHED. THESE CONVERSIONS ARE COMPARED WITH THE COMPARISON CHART IN TABLE I, GIVEN AS ERRORS IN D VALUES.

μ(MPa)	Duro A	Duro D (Simulated)	Duro D (from Table I)	Error
3.30	75	25	24	4%
6.0	85	32	29	10%
9.20	90	40	35	14%

CORRELATION BETWEEN GAUSSIAN ELASTIC MODULUS AND HARDNESS

Figure 10 shows the relationship between the elastic modulus E_0 by Equation (9a) for the Gaussian model vs shore hardness A obtained by finite element simulations. The Gent predictions, and the Briscoe/Sebastian predictions are also presented for comparison purposes. In Figure 10, all predictions give the same trend for the relation between E_0 and shore A hardness. However, the fully nonlinear analysis generally gives a higher prediction of elastic modulus for a given hardness than the other three predictions. Figure 11 shows the difference between the

elastic modulus predicted by the fully nonlinear analyses and those predicted by the other two theories, given as deviations from the fully nonlinear analyses. The difference between the Briscoe/Sebastian theory and the fully nonlinear model ranges from 18% to 10% and shrinks as the hardness increases, since the deviation of their theory from the fully nonlinear analyses becomes smaller as the penetration of the indentor decreases due to the increasing stiffness of the elastomer. However, a different trend is observed in the difference between the Gent theory and the fully nonlinear analyses. The reason for this trend is because the Gent theory used the average diameter of the upper and lower surface of the truncated cone indentor as the diameter of the equivalent flat punch, whose deviation from the reality is pronounced as the penetration decreases.

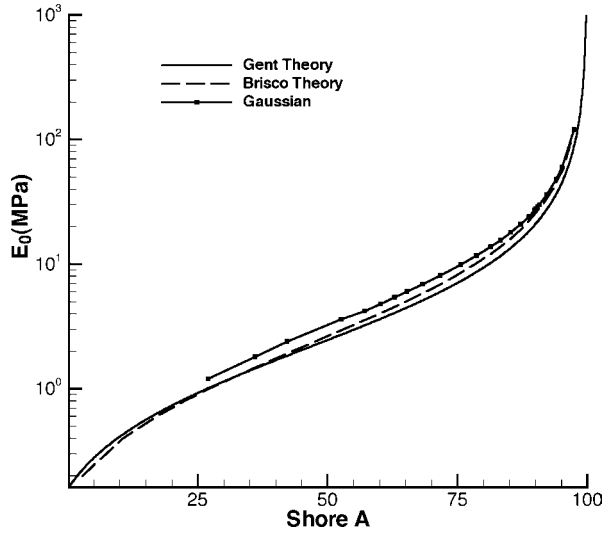

FIG. 10. — Relations between Shore A hardness and initial elastic moduli of elastomeric materials.

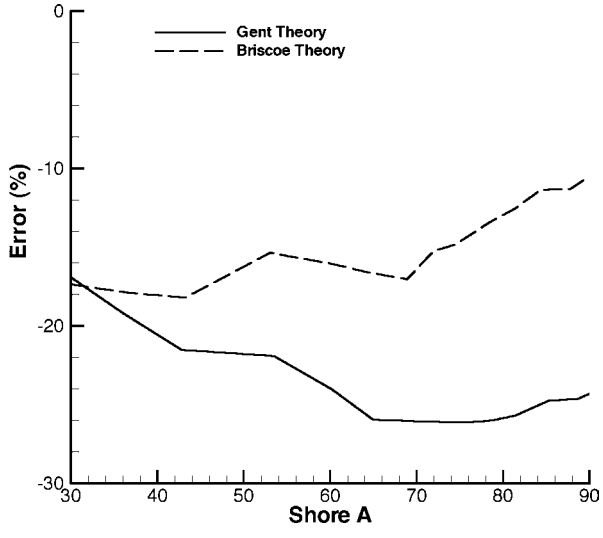

FIG. 11. — The differences of the elastic modulus for the given hardness between the finite element analyses and the other theories, given as deviation from the finite element analyses.

A first order estimation for type D durometer hardness can be obtained using the linear elastic solution.[13] For the cone indentor, the normal force on the indentor is

$$F_r^D = \frac{2E}{\pi\left(1-\nu^2\right)}\tan\theta h^2 \tag{10}$$

Combining with Equation (5b), the relation between elastic modulus and durometer D hardness for $\theta = 15°$, $\nu = 0.5$, is

$$H_D = 100 - \frac{20\left(-78.188 + \sqrt{6113.36 + 781.88E}\right)}{E} \tag{11}$$

Figure 12 shows the comparison between simulated results and the first order approximations to D scale hardness. The two predictions give the same trend between the relation of elastic modulus and shore hardness D. However, the fully nonlinear analysis generally gives lower elastic modulus prediction than the linear elastic theory for a given hardness. The difference increases as the hardness increases.

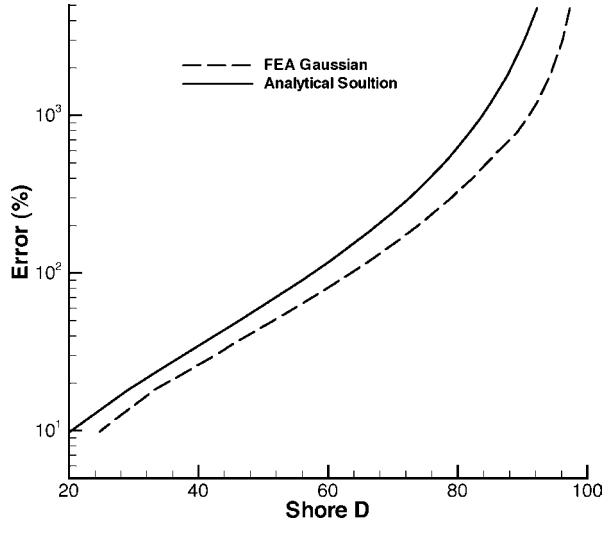

FIG. 12. — The relation between Shore D hardness and initial elastic moduli of elastomeric and elastomeric-like materials.

Figure 13 shows the relationship between elastic modulus and Shore A/Shore D hardness, given by finite element simulations. For both hardness scales, the logarithm of elastic modulus is proportional to the hardness values in the range of 20A(D) to 80A(D). The region where the two scales overlap corresponds to a linear region for Shore D, but mostly nonlinear region for Shore A. When the overlap is in the linear region for both scales, good conversions can be obtained, as for 75A to 25D; whereas when the overlap occurs in linear vs nonlinear regions, the conversions become worse, as for 90A to 40D, since the logarithm of the elastic modulus varies with Shore A values in a much faster rate than it does with Shore D values.

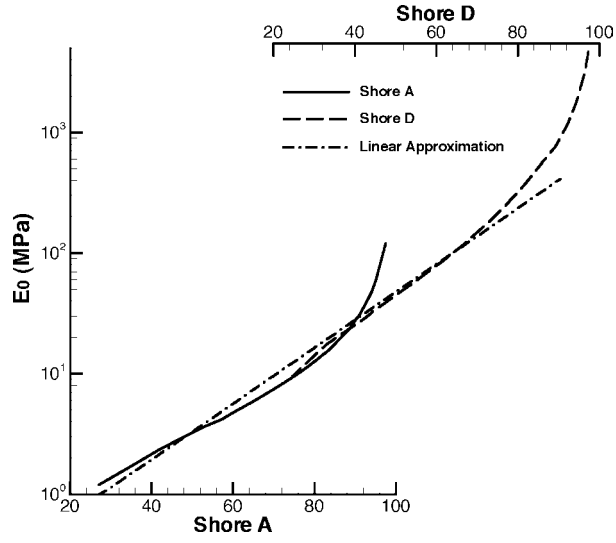

FIG. 13. — The relations between elastic modulus and Shore A/Shore D hardness for elastomeric and elastomeric-like materials, given by finite element simulations. The linear approximation is given by Equation (20).

It is also noted that there exists an almost linear relation between the logarithm of elastic modulus and a hardness scale

$$\log E_0 = 0.0235S - 0.6403 \tag{12a}$$

$$S = \begin{cases} Shore\ A & 20A < S < 80A \\ Shore\ D + 50 & 80A < S < 85D \end{cases} \tag{12b}$$

LIMITING EXTENSIBILITY EFFECT

As seen from Figure 8(b), large chain stretches can develop during the indentation process. For materials having small limiting extensibilities, this large chain stretch could be close to its locking stretch. Therefore, it is important to evaluate the effect of chain extensibility on the durometer hardness. Since the Arruda-Boyce material model captures the limiting extensibility of elastomeric materials, it is used in this section and then compared to the results that had been obtained using the Gaussian model.

Figure 14 depicts the tensile stress vs stretch curve for the Arruda-Boyce materials with $\mu = 1.35MPa$ and with various N values ranging from $N = 2$ to $N = 100$. At small stretches, the initial modulus for the material with smaller N is larger (Equation (9b)); At large stretches, the stiffness of the material with smaller N increases dramatically. Note that $N = 100$ corresponds to a limiting chain extensibility of $\lambda_L = 10$ and the upturn of the stress stretch curve occurs at an axial stretch of about 17, and $N = 4$ corresponds to a limiting chain extensibility of $\lambda_L = 2$ and the upturn occurs at an axial stretch of about 3.4. Note that the chain limiting extensibility is significantly lower than the limiting extension of the sample observed in a uniaxial tensile test because the molecular chains in the underlying molecular network accommodate macroscopic deformation through both chain stretching and chain rotation.

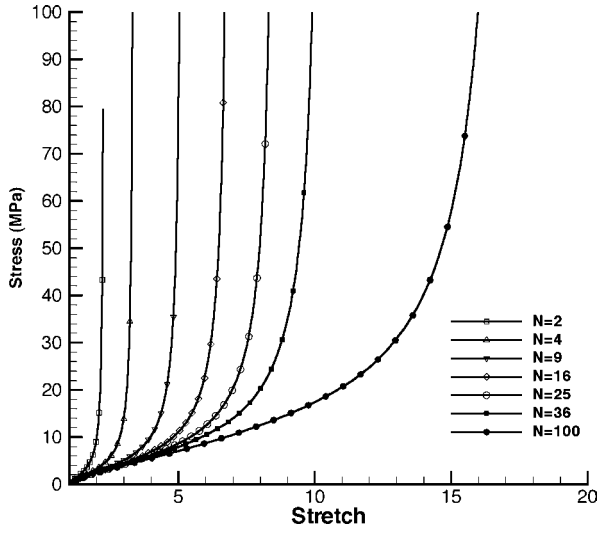

FIG. 14. — The stress-stretch curves for $\mu = 1.35MPa$ and different Ns of the Arruda-Boyce model.

Figure 15 shows the dependence of the durometer hardness vs limiting chain extensibility, N, for $\mu = 1.35MPa$, $\mu = 0.75MPa$ and $\mu = 0.35MPa$. The corresponding Gaussian result with the same E_0 is also presented. For N smaller than about 25 (corresponding to a limiting chain extensibility of $\lambda_L = 5$ and uniaxial tensile stretch of $\lambda = 8.5$), the predictions which account for the non-Gaussian behavior of the elastomer begin to deviate from those using the Gaussian material model and are substantially higher than those of the Gaussian material as N decreases. These higher hardness predictions are not purely a result of the effect of N on the initial modulus since the simulations using the Gaussian model with the same initial E_0 give lower predictions of hardness. The higher hardness prediction also result from the durometer test applying stretches that approach the limiting chain extensibility for cases when N is less than 25.

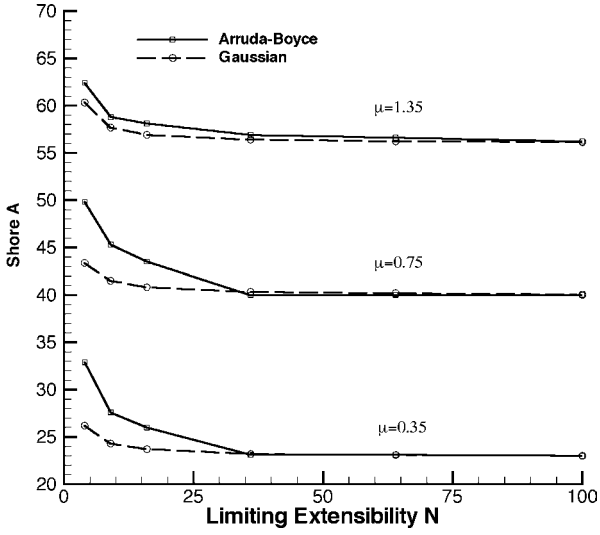

FIG. 15. — The solid lines show the dependence of the durometer A hardness vs N for $\mu = 1.35MPa$, $\mu = 0.75MPa$ and $\mu = 0.35MPa$. The corresponding Gaussian results with the same E_0 are also presented as the dashed lines.

The effect of the limiting extensibility is also influenced by μ. As shown in Figure 15, when μ is small, large chain stretch can develop during indentation, the effect of the limiting extensibility is pronounced. When μ increases, the penetration of the indentor becomes small. Hence, the molecular chains are unlikely to be stretched close to their locking stretch, and the effect of the limiting extensibility is reduced. As shown in Table III, when $\mu = 2.95MPa$, the difference in Shore A hardness is less than 5% when N varies from 4 to 100. Therefore, it is more likely that when λ_L is less than 5 and μ is less than $2MPa$ the effect of the chain limiting extensibility is important. Note that limiting extensibilities significantly less than 5 are quite common in soft biological tissues[8,14] as well as in elastomers.

TABLE III
PREDICTIONS OF DUROMETER A HARDNESS FOR DIFFERENT COMBINATIONS OF μ AND N IN THE ARRUDA-BOYCE MODEL

		N				
		4	9	16	36	64
μ(MPa)	0.35	32.9	27.6	26.0	23.1	23.1
	0.55	42.9	37.9	35.8	31.6	31.6
	0.75	49.8	45.3	43.5	40.0	40.0
	0.95	54.9	50.9	49.9	48.5	48.5
	1.35	62.4	58.8	58.1	56.9	56.6
	1.75	67.7	64.6	63.6	63.1	62.5
	2.15	71.8	68.9	68.2	67.3	67.1
	2.55	74.9	72.4	71.8	70.9	70.7
	2.95	77.5	75.2	74.5	73.7	73.6
	3.35	79.6	77.5	77.0	76.3	76.1
	3.75	81.4	79.4	78.9	78.2	78.2
	4.15	82.9	81.1	80.4	80.0	79.9
	4.45	83.8	82.1	81.6	81.2	81.0
	5.0	85.4	83.8	83.3	83.0	82.8
	5.0	86.6	85.1	84.7	84.3	84.2
	6.0	87.6	86.2	85.8	85.5	85.4
	9.0	91.4	90.5	90.2	90.0	89.9
	12.0	93.4	92.7	92.4	92.3	92.2

Table III gives predictions of Shore hardness A for different combinations of μ and N in the Arruda-Boyce model. In Table III, different combinations of N and μ may lead to the same predicted durometer hardness. Table IV gives two examples of N and μ pairs which lead to Shore 73.6A. The corresponding initial elastic moduli are also listed in Table IV. Although the materials have the same durometer hardness, their elastic moduli are different by about 5%. It is therefore important to notice that predicting elastic moduli from durometer tests sometimes gives ambiguous results due to the limiting extensibility of the chain. There does not exist a one-to-one mapping between the initial elastic modulus and durometer hardness.

TABLE IV
MATERIALS WITH DIFFERENT MATERIAL PARAMETERS HAVE SAME DUROMETER HARDNESS

N	μ(MPa)	Duro (A)	E_0 (MPa)
5.76	2.55	73.6	8.59
36	2.95	73.6	9.01

In the applications of durometer hardness, many researchers assume that larger durometer hardness corresponds to larger elastic modulus but less extensibility. However, one should be cautious when making this inference. For instance, considering two combinations of μ and N in the Arruda-Boyce model in Table V, the second combination gives larger durometer hardness, but has higher extensibility as well, as it can be seen from the stress-stretch curves (Figure 16).

TABLE V
MATERIAL WITH HIGHER DUROMETER HARDNESS AND HIGHER ELASTIC MODULUS CAN HAVE HIGHER EXTENSIBILITY

N	μ(MPa)	E_0(MPa)	Duro (A)	Maximum extension
9	0.95	3.06	50.9	480%
16	2.55	7.95	71.8	690%

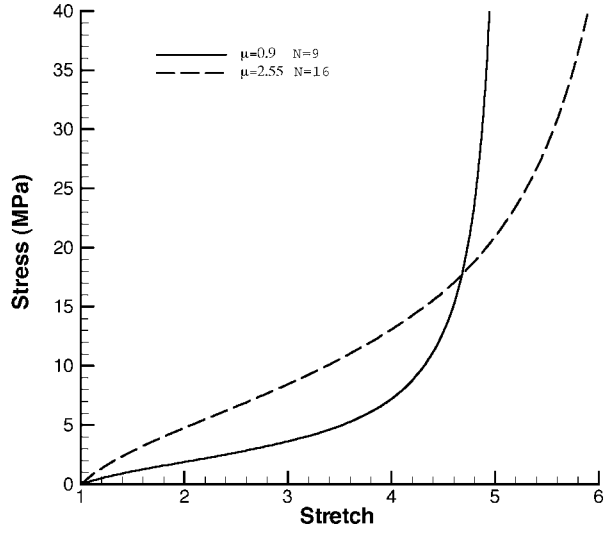

FIG. 16. — The stress-stretch curves for two different Arruda-Boyce materials. The material with μ = 2.55*MPa* and N = 16 has larger initial elastic modulus and larger extensibility.

CONCLUSIONS

Durometer hardness tests were analyzed using fully nonlinear finite element simulations accounting for both material and geometrical nonlinearities. The simulation results are verified by matching the predicted durometer hardness in scale D with ASTM D 2240 for the Gaussian material with the given durometer hardness in scale A. The relations between elastic modulus and the durometer hardness A scale and D scale are provided. The fully nonlinear finite element analyses predict higher values of the elastic modulus than those given by the Gent theory and the Briscoe/Sebastian theory. The influence of the limiting extensibility of the elastomer is evaluated using the non-Gaussian Arruda-Boyce eight-chain model. The chain extensibility eliminates the one-to-one mapping between the elastic modulus and the durometer hardness. The limiting

extensibility also increases the reaction force to the indentation and thus increases the hardness of the material. This effect is pronounced as the chain extensibility decreases to values of λ_L less than 5, particularly when μ is less than *2MPa*. These results indicate that the durometer hardness test can be used to provide a reasonable approximation (the error is generally less than 5% for large λ_L and μ) to the initial neo-Hookean modulus using the plot of Figure 13 or Equation (12), however care must be used if the limiting extensibility is known to be small. The mapping does not address the time dependence of the material behavior, the initial yield-like phenomenon present in thermoplastic elastomers, or the initial anisotropy existing in many soft tissues. However, it does provide the framework for exploring such complexities in future work.

REFERENCES

[1]ASTM Designation, D 2240-97.

[2]ASTM Designation, D1415-88.

[3]V. Falanga, B. Bucalo, *J. Ameri. Acad. Dermatol.* **29**, 47 (1993).

[4]P. L. Reisfeld, *J. Ameri. Acad. Dermatol.* **31**, 515 (1994).

[5]J. O. Ladeji-Osias, N. A. Langrana, Proc. 22nd Ann. EMBS Inter. Conf., July 23-28, 2000, Chicago, IL, pp 2114-2117.

[6]A. N. Gent, *Trans. Inst. Rubber Ind*. **34**, 46 (1958).

[7]B. Brsicoe, K. S. Sebastian, RUBBER CHEM. TECHNOL. **66**, 837 (1993).

[8]J. E. Bischoff, E. M. Arruda, K. Grosh, *J. Biomech*. **33**, 645 (2000).

[9]W. V. Chang, and S. C. Sun, RUBBER CHEM. TECHNOL. **64**, 202 (1991).

[10]L. R. G. Treloar, "The Physics of Rubber Elasticity," Oxford University Press, Oxford, 1975.

[11]E. M. Arruda, M. C. Boyce, *J. Mech. Phys. Solids* **41,** 389 (1993).

[12]D. J. T. Hill, M. I. Killen, *et al.*, *Wear* **208,** 155 (1997).

[13]I. N. Sneddon, *Int. J. Eng. Sci.* **3**, 47 (1965).

[14]Y. C. Fung, "Biomechanics: mechanical properties of living tissues," Springer-Verlag, New York, 1993.

[*Received March 2002; revised July 2002*]